Chapter 5

Beam monitoring: analysis and results

5.1 Overview

With the new high-intensity accelerator beam facilities becoming more and more powerful, while attempting measurements at increasingly high precision, real time beam monitoring is becoming essential, both to protect equipment, and to precisely measure beam properties. The simulations and analysis performed for this thesis aim to evaluate the beam monitoring capabilities of SAND for the NuMi muon neutrino beam.
Many of the beam characteristics can be used for beam monitoring. For this study we have considered the reconstructed energy of muons produced in ν_μ CC interactions in SAND's electro-magnetic calorimeter. The neutrino interactions were simulated using the GENIE neutrino MonteCarlo generator according to the ν_μ spectrum and CC/NC interaction rates reported in Figure 4.1. In particular, the interactions were all generated to have vertex in one of the eight frontal barrel calorimeter modules. The particles produced in the interactions were then propagated using edep-sim. The ECAL and STT signals were then digitized and the clusters and tracks reconstructed. Note that in order to shorten the simulation times the digitization and reconstruction steps were performed only on the primary particles of the interactions.
No particle identification has been implemented for SAND's simulation chain at the time of writing. The muon tracks where thus selected post reconstruction from the MonteCarlo truth PID informations. In order to select only the muons produced in CC interactions in the inner layers of calorimeter, a selection on the energy deposition on the outer layer of the ECAL was implemented. The energy of the muons that passed the outer layer cut was

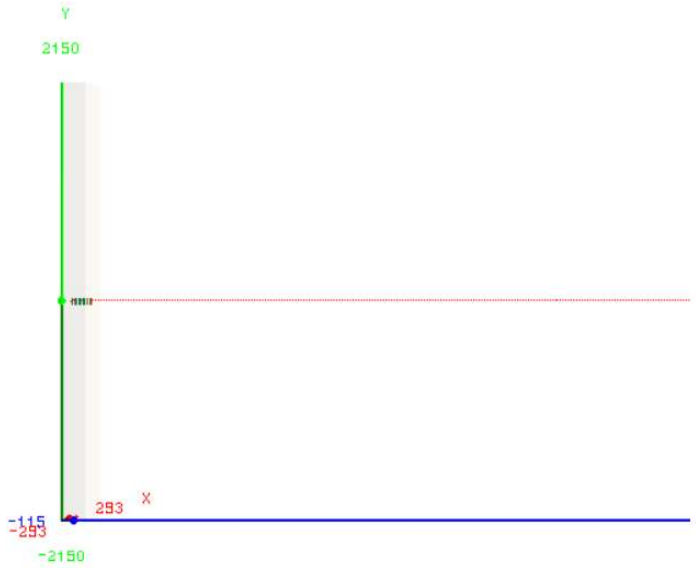

Figure 5.1: A 10 GeV muon hitting a calorimeter module simulated using the edep-sim GEANT4 particle gun option and drawn using edep-disp. The red line indicates the muon track, with the hits inside the calorimeter highlighted in green. The coordinates are in millimeters.

then reconstructed from the STT track fit information as described in Section 4.5.2.
The shape of the reconstructed energy spectrum of the muons produced in CC interactions, depends on the original ν_μ energy spectrum. Any anomalies in the beam production would thus in principle cause variations in both spectra. We study the sensitivity to these anomalies by applying two-sample homogeneity tests on the reconstructed muon energy distributions.

5.2 Preliminary measurements

In order to perform the energy spectrum measurements needed for the beam monitoring quality evaluation, a series of preliminary measurements were needed. Firstly we needed to extrapolate the calibration coefficient between the energy loss of a muon in a calorimeter module cell and the total number of photo-electrons produced on the PMs' photo-cathodes and counted by the ADCs. This was essential to be able to set the p.e. threshold used for the outer layer cut.
An evaluation of the efficacy of the cut in selecting the muons not having a

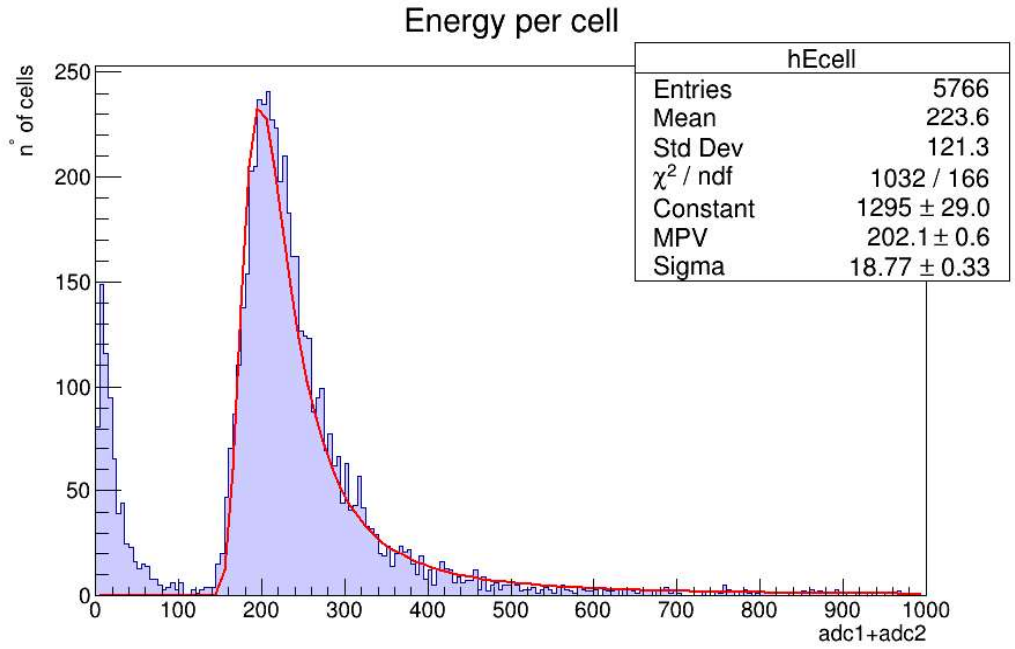

Figure 5.2: Distribution of total number of photo-electrons produced at the passage of a 10 GeV muon in a ECAL cell. The histogram has been produced from a set of 1000 muons simulated hitting a calorimeter module. These were generated using the GEANT4 particle gun mode implemented in edep-sim. The red line indicates a Landau fit, the results of which are summarized in the box in the upper right corner of the histogram canvas.

vertex in the outer layer was also needed, together with measurements of the STT track fitting algorithm efficiency and the quality of the muon energy reconstruction.

5.2.1 Muon energy loss calibration

In order to measure the calibration constant between the muon energy loss we simulated a set of 1000 muons with an initial energy of 10 GeV, hitting a calorimeter barrel module at the centre of its smaller base. The muons were generated using a simple GEANT4 particle gun via $edep - sim$, while the geometry containing the single calorimeter module was produced using *gegede* exactly in the same way as for the entire ECAL. A graphical representation of one of these events is shown in Figure 5.1. Both the particle gun and the module were placed in vacuum.

The hits and relative energy losses were then assigned to the calorimeter

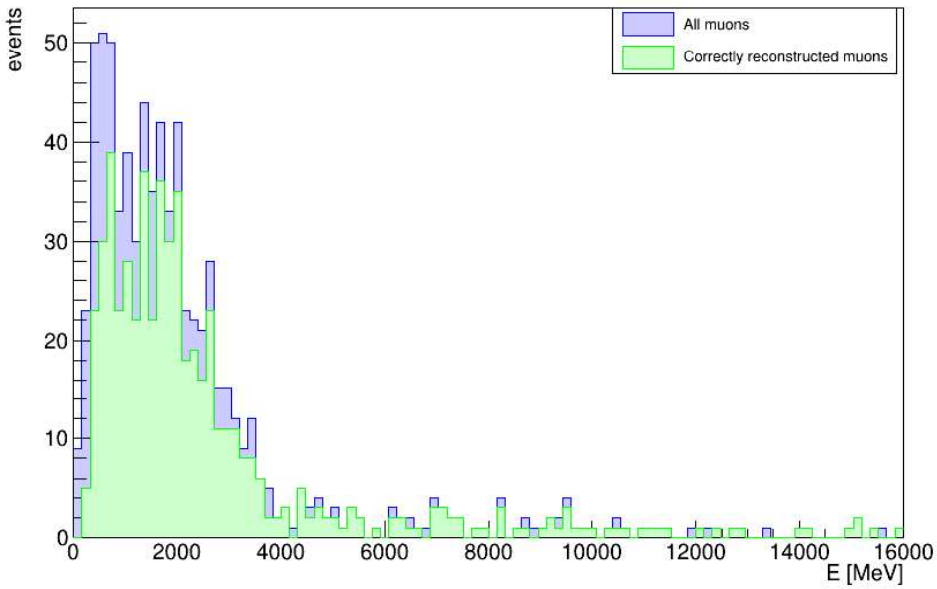

Figure 5.3: Energy (Montecarlo truth) distribution of muons produced in CC events in the front calorimeters of SAND. The histogram in blue contains all the simulated muons, while the one in green contains only the ones for which the reconstruction was successful.

cells during digitization thus producing two ADC values for each cell. The distribution of the sum of the two ADC values for each cell, which in our simple digitization algorithm corresponds with the total production of photo-electrons, is shown in Figure 5.2. Performing a Landau fit on the histogram we find that the most probable value is given by $N_{p.e.}^{cell} = (202.1 \pm 0.6)$.
To produce an estimate of the energy loss in MeV of a muon traversing the cell, we can consider a minimum ionizing particle (MIP) traversing 40 slabs of lead for a total of $\Delta x_{Pb} = 1.6$ cm and 40 slabs of plastic scintillator for a total thickness of $\Delta x_{Sc} = 2.8$ cm. In this approximation, a rough estimate of the energy loss can be given by:

$$\Delta E_{cell} \simeq \left(\frac{dE}{dx}\right)_{Pb}^{MIP} \Delta x_{Pb} + \left(\frac{dE}{dx}\right)_{Sc}^{MIP} \Delta x_{Sc} \simeq 40\text{MeV} \qquad (5.1)$$

where the dE/dx values are taken to be approximately 12.74 Mev/cm in lead and 2.74 Mev/cm in the scintillator.
The average number of photo-electrons produced in a cell per MeV of energy

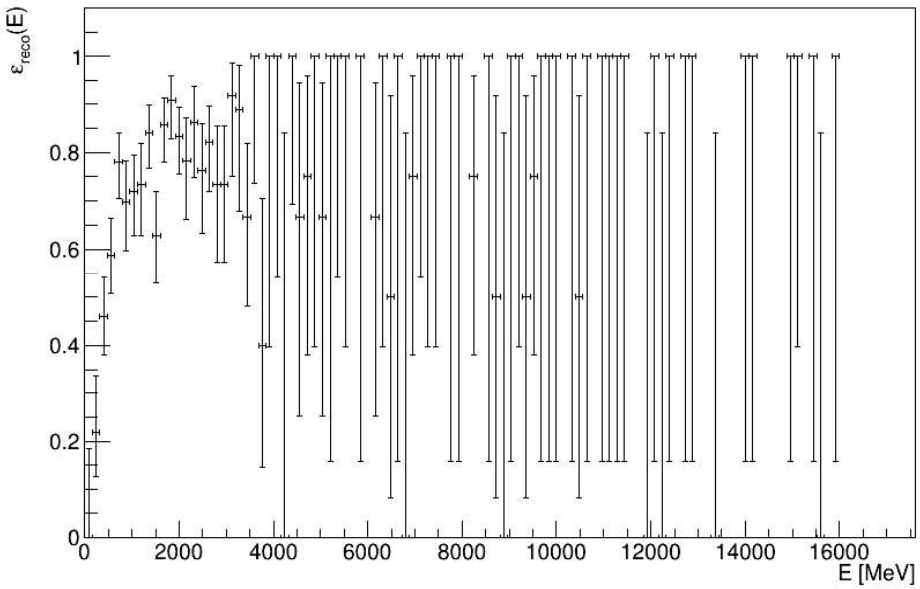

Figure 5.4: Reconstruction algorithm efficiency asa function of the muon energy from the Montecarlo truth.

deposited by a muon is thus roughly given by the calibration coefficient:

$$c = \frac{N_{p.e.}^{cell}}{\Delta E_{cell}} \simeq 5 \text{ [p.e./Mev]} \tag{5.2}$$

5.2.2 Muon track reconstruction efficiency

The STT track reconstruction algorithm described in Section 4.5 can sometimes fail. If either one of the two fits fail, the reconstruction is considered unsuccessful and the event is flagged and discarded for the final energy reconstruction.
The circular fit is considered not successful if the track has less than three hits on horizontal straw tubes or if problems occurred in assigning the coordinate values to any of the straw hits or in any of the passages of the fit algorithm (like for example having a 0 value as a denominator). The linear fit always fails if the circular fit is unsuccessful, since it necessitates the (y_C, z_C) and R estimates in order to calculate the ρ coordinates. The other failure conditions are analogous to the circular fit ones, with additional problems occurring when extrapolating the y coordinate from the x and z values obtained from the vertical straws.

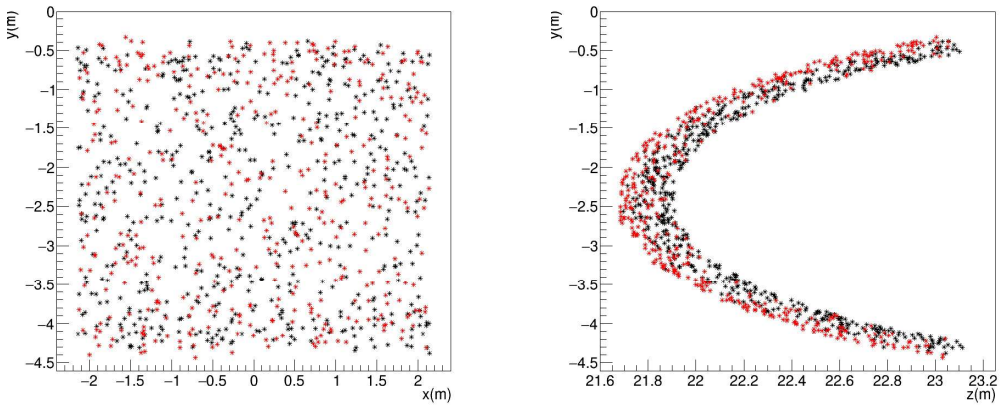

(a) (b)

Figure 5.5: Spatial distribution in ND hall global coordinates of the neutrino interaction vertexes of the events that survive the outer layer cut (black) and the events having their vertex in the outer layer from the Montecarlo truth (red). The two panels show the projection (a) on the xy plane and (b) on the yz plane.

In order to evaluate the efficiency of the reconstruction algorithm we performed a complete simulation for 1000 ν_μ events on the front calorimeter modules. We then filed two histograms of the muon energy distribution from the Montecarlo truth: one containing all the muons produced in CC interactions and one only the muons for which the reconstruction was successful (Figure 5.3).
The reconstruction efficiency as a function of energy is given by the ratio between the number of successfully reconstructed muons at a certain energy N^{reco}_{muon} and the total number of muons N_{muon} :

$$\varepsilon_{reco}(E) = \frac{N^{reco}_{muon}(E)}{N_{muon}(E)} \tag{5.3}$$

The reconstruction efficiency distribution can be obtained by dividing each bin content value from the two histograms one by one. The result of this operation is shown in Figure 5.4.

5.2.3 Selection on the outer layers

Before proceeding with the energy reconstruction we would like to discard from the analysis, muons that are not the product of ν_μ CC interactions

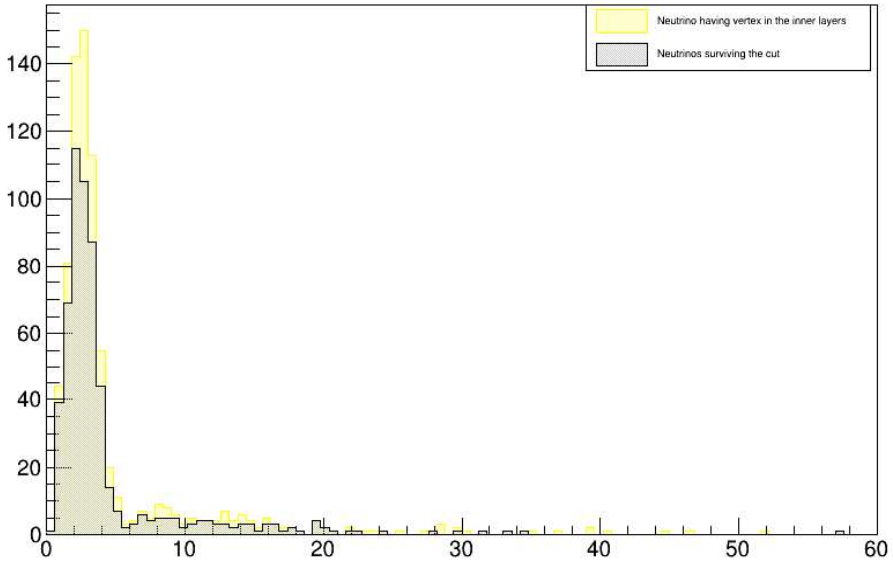

Figure 5.6: Energy (Montecarlo truth) distribution of neutrinos having their interaction vertex in one of the 4 inner layers (yellow); Energy (Montecarlo truth) distribution of neutrinos surviving the outer layer energy cut (gray).

in the front calorimeter modules and that are thus produced outside the detector (either in the neutrino beam or from cosmic rays). Doing so we will also exclude the ν_μ having their interaction vertex in the outer layer of the detector's ECAL modules.

We then introduce an energy deposition threshold on the outer layer of $\Delta E_{th} = 15$ MeV. Using the conversion coefficient found in Section 5.2.1 we then find the threshold in number of photo-electron production:

$$N_{p.e.}^{th} = c \times \Delta E_{th} = 75 \text{ p.e.} \tag{5.4}$$

Any event having photo-electron production in the outer layer ≥ 75 p.e. is thus eliminated. Since in our simulation no externally produced muons are considered, the only events that should be eliminated are the ones having their interaction vertex on the outer layer.
In Figure 5.5 we show the spacial distribution of the interaction vertexes of the events surviving the cut in black, together with the events having their vertex in the outer layer in red. In Figure 5.6 we show the distribution in neutrino energy from the Montecarlo truth of the events having vertex in one of the four inner layers in the detector (yellow) and the ones surviving the

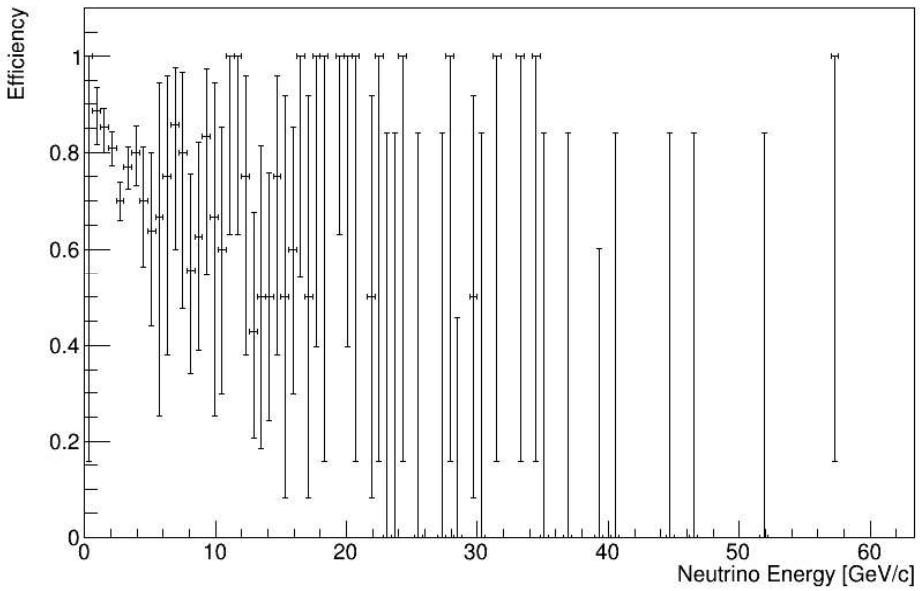

Figure 5.7: Selection efficiency as a function of neutrino energy from the Montecarlo truth.

selection (gray).
We can define now the cut efficiency as the ratio between the events surviving the selection N_{cut} and the total number of events having a vertex in the inner layers N_{inner} as a function of energy:

$$\varepsilon_{cut}(E) = \frac{N_{cut}(E)}{N_{inner}(E)} \tag{5.5}$$

The selection efficiency distribution can also be obtained by dividing each bin content value from the two histograms one by one and is shown in Figure 5.7.

5.3 Two-sample statistical tests

In order to understand if we can spot an anomaly in the neutrino beam production, we would like to test if the modified muon energy spectrum is not consistent with the original one i.e. if the hypothesis that the two histograms are sampled from the same distributions is incorrect. We do not have a clearly defined null hypothesis for what the common distribution would be, so we can only compare the two histograms bin by bin with a so called two-sample

statistical test. Of the many possible tests that exist we considered three: the simple χ^2 test in the large sample approximation, the Kolmogorov-Smirnov test and the Anderson-Darling test.

5.3.1 Approximated χ^2 test

Given two histograms with the same number of bins k and boundaries, the bin contents are the realisations of two random variables U and V. If we call u_i and v_i the realizations of the bin contents and μ_i and ν_i, the bin contents distributions have the shapes of Poisson functions. The sampling distributions of the two histograms are thus:

$$P(U = u) = \prod_{i=1}^{k} \frac{\mu_i^{u_i}}{u_i!} e^{-\mu_i} \tag{5.6}$$

$$P(V = v) = \prod_{i=1}^{k} \frac{\nu_i^{v_i}}{v_i!} e^{-\nu_i} \tag{5.7}$$

The hypothesis that the two histograms follow the same distribution is equivalent to saying that there are k constants p_i that are the probabilities of belonging to the ith bin for both histograms, so that:

$$\sum_{i=1}^{k} p_i \tag{5.8}$$

Given the total number of entries for each histogram $N_u = \sum u_i$ and $N_v = \sum v_i$, then the probability of observing u_i events in the ith bin of the first histogram and the probability of observing v_i events in the ith bin of the second histogram given by:

$$\frac{e^{-N_u p_i}(N_u p_i)^{u_i}}{u_i!} \tag{5.9}$$

$$\frac{e^{-N_v p_i}(N_v p_i)^{v_i}}{v_i!} \tag{5.10}$$

If the hypothesis of compatibility between the two histograms is correct the maximum likelihood estimator of p_i is:

$$\hat{p}_i = \frac{u_i + v_i}{N_u + N_v} \tag{5.11}$$

We can then construct the test statistic:

$$T = \sum_{i=1}^{k} \frac{(u_i - N_u\hat{p}_i)^2}{N_u\hat{p}_i} + \sum_{i=1}^{k} \frac{(v_i - N_v\hat{p}_i)^2}{N_v\hat{p}_i} = \frac{1}{N_u M_v} \sum_{i=1}^{k} \frac{(N_u u_i - N_v v_i)^2}{u_i + v_i} \tag{5.12}$$

T follows approximately a χ^2 distribution for $k-1$ degrees of freedom, as long as we are in a situation where the two samples are large enough that the bin contents are distributed normally. We can thus estimate from the χ^2 distribution, the p-value, which in this case is the probability of having two histograms that are as much or less in agreement than the ones we are testing, if they are sampled from the same distribution.

5.3.2 Kolmogorov-Smirnov test

The two-sample Kolmogorov-Smirnov test consists in measuring the maximum difference between the two cumulative distribution functions (CDFs) and compare with the null homogeneity hypothesis expectations.
We approximate the cumulative distribution functions as histograms:

$$u_{ci} = \sum_{j=1}^{i} u_j/N_u \tag{5.13}$$

$$v_{ci} = \sum_{j=1}^{i} v_j/N_v \tag{5.14}$$

The test statistic is then given by:

$$T_{KS} = \max_i |u_{ci} - v_{ci}| \tag{5.15}$$

The null hypothesis is rejected at significance level α if:

$$T_{KS} \geq c(\alpha)\sqrt{\frac{N_u + N_v}{N_u \cdot N_v}} \tag{5.16}$$

where $c(\alpha)$ is the inverse of the Kolmogorov distribution and in general can be calculated approximately as:

$$c(\alpha) = \sqrt{-\ln(\alpha/2) \cdot (1/2)} \tag{5.17}$$

Note that the Kolmogorov-Smirnoff test tends to emphasize differences near the peak of the distribution, where the largest fluctuations are expected for Poisson probabilities.

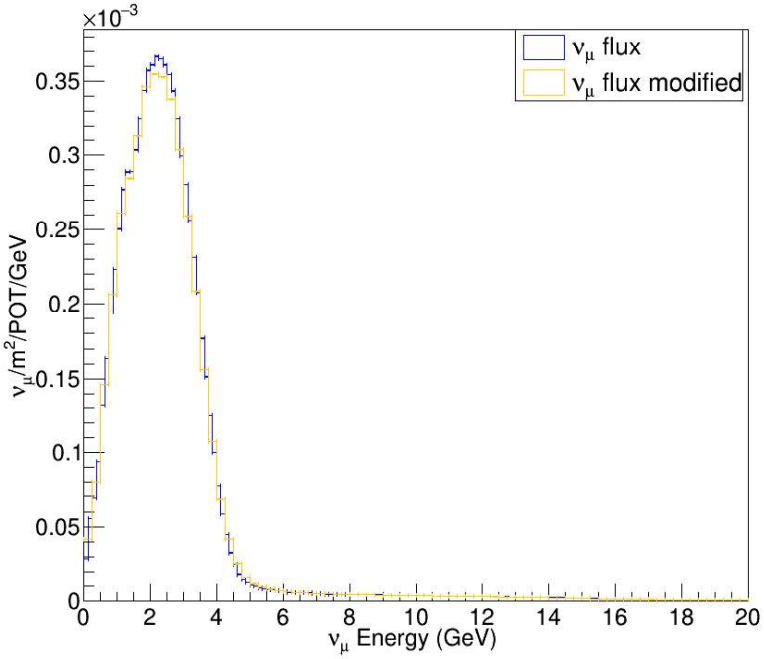

Figure 5.8: (Blue) Muon neutrino flux as a function of neutrino energy produced by the Numi neutrino beam in standard conditions (Orange) Muon neutrino flux as a function of neutrino energy generated when the second horn had a transverse displacement of +0.05mm in the Y coordinate.

5.3.3 The Anderson-Darling test

The Anderson-Darling test is a modified version of the Kolmogorov-Smirnov test design to improve the sensitivity to the tails of the CDFs. The original statistical test, designed to test the compatibility of a data set x having an empirical CDF $F_m(x)$, with a continuous distribution, having the CDF $F_0(x)$ under the null hypothesis is:

$$A_m^2 = m \int_{-\inf}^{\inf} \frac{[F_m(x) - F_0(x)]^2}{F_0(x)[1 - F_0(x)]} dF_0(x) \tag{5.18}$$

Scholz and Stephens adapted this statistic to the k-sample case, which in our simple two-sample situation reads:

$$T_{AD} = \frac{1}{N_u + N_v} \sum_{j=k_{min}}^{k_{max}-1} \frac{u_j + v_j}{\Sigma_j (N_u + N_v - \Sigma_j)} \times \left[((N_u + N_v)\Sigma_{uj} - N_u \Sigma_j)^2 / N_u + ((N_u + N_v)\Sigma_{vj} - N_v \Sigma_j)^2 / N_v \right] \tag{5.19}$$

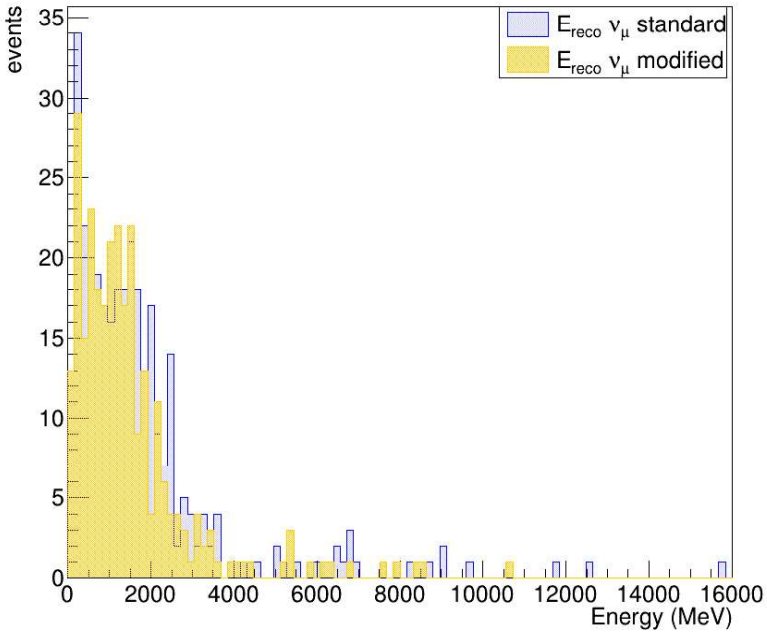

Figure 5.9: (Blue) Muon neutrino flux as a function of neutrino energy produced by the Numi neutrino beam in standard conditions (Orange) Muon neutrino flux as a function of neutrino energy generated when the second horn had a transverse displacement of +0.05mm in the Y coordinate.

where k_{min} is the first non-zero bin for both histograms, k_{max} is the number of bins until the last non-zero bin and:

$$\Sigma_{uj} = \sum_{i=1}^{j} u_i; \quad \Sigma_{uj} = \sum_{i=1}^{j} u_i; \tag{5.20}$$

$$\Sigma_j = \sum_{i=1}^{j} (u_i + v_i) = \Sigma_{uj} + \Sigma_{vj} \tag{5.21}$$

5.4 Beam monitoring measure

For the beam monitoring measure we considered the muon neutrino flux produced by the NuMi neutrino beam in standard conditions and we confronted it with the one generated when the second horn had a transverse displacement of +0.05mm in the Y coordinate. The corresponding neutrino fluxes simulated by the NuMi collaborations as a function of energy in units

of $\nu_\mu/m^2/POT/\text{GeV}$ are shown in Figure 5.8.
Note that the ν_μ fluxes were also generated by the collaboration with modifications to many other critical parameters. These include: transverse displacement in both horns and the proton beam; modifications in the proton beam radius and angle on target; shifts in the values of the decay pipe radius, horn currents, target density and horn water layer thickness. The critical parameter for this study has been selected arbitrarily and is not of special interest over any of the others.
Using the neutrino fluxes, we simulated using GENIE two sets of interactions in the front calorimeter, in the number that we expect for a week of beam running, as suggested by the ND collaboration for beam monitoring measures. Given the number of interactions per second expected in a calorimeter module ϵ, and the number of target modules $n_{mod} = 10$ this corresponds to:

$$N_{week} = \epsilon \times n_{mod} \times 3600 \times 7 \simeq 1.7 \times 10^6 \tag{5.22}$$

Following the simulation chain, we used edep-sim to propagate the particles produced in the interactions, we digitized the signal, reconstructed the tracks and the energies of the muons produced in the CC interactions and applied the energy selection on the outer layer of the calorimeter. The reconstructed energy distributions of the muons for which all the simulation steps were successful are shown in Figure 5.9 for both samples.
Applying the three statistical tests discussed in Section 5.3, we find that the probabilities of having two energy distributions that are as in agreement or worse, under the null hypothesis that they are both derived from the same statistical distribution (i.e. the p-value) are:

$$\begin{aligned} \text{p-value} &= 0.384572 \ (\chi^2); \\ &= 0.087786 \ \text{(Kolmogorov-Smirnov)}; \\ &= 0.102824 \ \text{(Anderson-Darling)}; \end{aligned} \tag{5.23}$$

The chi-square test was performed on the histograms, while the Kolmogorov-Smirnov and Anderson-Darling tests were applied to un-binned data.